Time-Dependent Searches for Point Sources of Neutrinos with the 40-String and 22-String Configurations of IceCube

IceCube Collaboration: R. Abbasi[1], Y. Abdou[2], T. Abu-Zayyad[3], J. Adams[4], J. A. Aguilar[1], M. Ahlers[5], K. Andeen[1], J. Auffenberg[6], X. Bai[7], M. Baker[1], S. W. Barwick[8], R. Bay[9], J. L. Bazo Alba[10], K. Beattie[11], J. J. Beatty[12,13], S. Bechet[14], J. K. Becker[15], K.-H. Becker[6], M. L. Benabderrahmane[10], S. BenZvi[1], J. Berdermann[10], P. Berghaus[1], D. Berley[16], E. Bernardini[10], D. Bertrand[14], D. Z. Besson[17], M. Bissok[18], E. Blaufuss[16], D. J. Boersma[18], C. Bohm[19], S. Böser[20], O. Botner[21], L. Bradley[22], J. Braun[1], S. Buitink[11], M. Carson[2], D. Chirkin[1], B. Christy[16], J. Clem[7], F. Clevermann[23], S. Cohen[24], C. Colnard[25], D. F. Cowen[22,26], M. V. D'Agostino[9], M. Danninger[19], J. C. Davis[12], C. De Clercq[27], L. Demirörs[24], O. Depaepe[27], F. Descamps[2], P. Desiati[1], G. de Vries-Uiterweerd[2], T. DeYoung[22], J. C. Díaz-Vélez[1], M. Dierckxsens[14], J. Dreyer[15], J. P. Dumm[1], M. R. Duvoort[28], R. Ehrlich[16], J. Eisch[1], R. W. Ellsworth[16], O. Engdegård[21], S. Euler[18], P. A. Evenson[7], O. Fadiran[29], A. R. Fazely[30], T. Feusels[2], K. Filimonov[9], C. Finley[19], M. M. Foerster[22], B. D. Fox[22], A. Franckowiak[20], R. Franke[10], T. K. Gaisser[7], J. Gallagher[31], M. Geisler[18], L. Gerhardt[11,9], L. Gladstone[1], T. Glüsenkamp[18], A. Goldschmidt[11], J. A. Goodman[16], D. Grant[32], T. Griesel[33], A. Groß[4,25], S. Grullon[1], M. Gurtner[6], C. Ha[22], A. Hallgren[21], F. Halzen[1], K. Han[4], K. Hanson[14,1], K. Helbing[6], P. Herquet[34], S. Hickford[4], G. C. Hill[1], K. D. Hoffman[16], A. Homeier[20], K. Hoshina[1], D. Hubert[27], W. Huelsnitz[16], J.-P. Hülß[18], P. O. Hulth[19], K. Hultqvist[19], S. Hussain[7], A. Ishihara[35], J. Jacobsen[1], G. S. Japaridze[29], H. Johansson[19], J. M. Joseph[11], K.-H. Kampert[6], T. Karg[6], A. Karle[1], J. L. Kelley[1], N. Kemming[36], P. Kenny[17], J. Kiryluk[11,9], F. Kislat[10], S. R. Klein[11,9], S. Knops[18], J.-H. Köhne[23], G. Kohnen[34], H. Kolanoski[36], L. Köpke[33], D. J. Koskinen[22], M. Kowalski[20], T. Kowarik[33], M. Krasberg[1], T. Krings[18], G. Kroll[33], K. Kuehn[12], T. Kuwabara[7], M. Labare[14], S. Lafebre[22], K. Laihem[18], H. Landsman[1], R. Lauer[10], R. Lehmann[36], D. Lennarz[18], J. Lünemann[33],

J. Madsen[3], P. Majumdar[10], A. Marotta[14], R. Maruyama[1], K. Mase[35], H. S. Matis[11], M. Matusik[6], K. Meagher[16], M. Merck[1], P. Mészáros[26,22], T. Meures[18], E. Middell[10], N. Milke[23], J. Miller[21], T. Montaruli[1,37], R. Morse[1], S. M. Movit[26], R. Nahnhauer[10], J. W. Nam[8], U. Naumann[6], P. Nießen[7], D. R. Nygren[11], S. Odrowski[25], A. Olivas[16], M. Olivo[21,15], A. O'Murchadha[1], M. Ono[35], S. Panknin[20], L. Paul[18], C. Pérez de los Heros[21], J. Petrovic[14], A. Piegsa[33], D. Pieloth[23], R. Porrata[9], J. Posselt[6], P. B. Price[9], M. Prikockis[22], G. T. Przybylski[11], K. Rawlins[38], P. Redl[16], E. Resconi[25], W. Rhode[23], M. Ribordy[24], A. Rizzo[27], J. P. Rodrigues[1], P. Roth[16], F. Rothmaier[33], C. Rott[12], C. Roucelle[25], T. Ruhe[23], D. Rutledge[22], B. Ruzybayev[7], D. Ryckbosch[2], H.-G. Sander[33], M. Santander[1], S. Sarkar[5], K. Schatto[33], S. Schlenstedt[10], T. Schmidt[16], A. Schukraft[18], A. Schultes[6], O. Schulz[25], M. Schunck[18], D. Seckel[7], B. Semburg[6], S. H. Seo[19], Y. Sestayo[25], S. Seunarine[39], A. Silvestri[8], A. Slipak[22], G. M. Spiczak[3], C. Spiering[10], M. Stamatikos[12,40], T. Stanev[7], G. Stephens[22], T. Stezelberger[11], R. G. Stokstad[11], S. Stoyanov[7], E. A. Strahler[27], T. Straszheim[16], G. W. Sullivan[16], Q. Swillens[14], H. Taavola[21], I. Taboada[41], A. Tamburro[3], O. Tarasova[10], A. Tepe[41], S. Ter-Antonyan[30], S. Tilav[7], P. A. Toale[22], S. Toscano[1], D. Tosi[10], D. Turčan[16], N. van Eijndhoven[27], J. Vandenbroucke[9], A. Van Overloop[2], J. van Santen[1], M. Voge[25], B. Voigt[10], C. Walck[19], T. Waldenmaier[36], M. Wallraff[18], M. Walter[10], Ch. Weaver[1], C. Wendt[1], S. Westerhoff[1], N. Whitehorn[1], K. Wiebe[33], C. H. Wiebusch[18], G. Wikström[19], D. R. Williams[42], R. Wischnewski[10], H. Wissing[16], M. Wolf[25], K. Woschnagg[9], C. Xu[7], X. W. Xu[30], G. Yodh[8], S. Yoshida[35], and P. Zarzhitsky[42]

[1]Dept. of Physics, University of Wisconsin, Madison, WI 53706, USA

[2]Dept. of Subatomic and Radiation Physics, University of Gent, B-9000 Gent, Belgium

[3]Dept. of Physics, University of Wisconsin, River Falls, WI 54022, USA

[4]Dept. of Physics and Astronomy, University of Canterbury, Private Bag 4800, Christchurch, New Zealand

[5]Dept. of Physics, University of Oxford, 1 Keble Road, Oxford OX1 3NP, UK

[6]Dept. of Physics, University of Wuppertal, D-42119 Wuppertal, Germany

[7]Bartol Research Institute and Department of Physics and Astronomy, University of Delaware, Newark, DE 19716, USA

[8]Dept. of Physics and Astronomy, University of California, Irvine, CA 92697, USA

[9]Dept. of Physics, University of California, Berkeley, CA 94720, USA

[10]DESY, D-15735 Zeuthen, Germany

[11]Lawrence Berkeley National Laboratory, Berkeley, CA 94720, USA

[12]Dept. of Physics and Center for Cosmology and Astro-Particle Physics, Ohio State University, Columbus, OH 43210, USA

[13]Dept. of Astronomy, Ohio State University, Columbus, OH 43210, USA

[14]Université Libre de Bruxelles, Science Faculty CP230, B-1050 Brussels, Belgium

[15]Fakultät für Physik & Astronomie, Ruhr-Universität Bochum, D-44780 Bochum, Germany

[16]Dept. of Physics, University of Maryland, College Park, MD 20742, USA

[17]Dept. of Physics and Astronomy, University of Kansas, Lawrence, KS 66045, USA

[18]III. Physikalisches Institut, RWTH Aachen University, D-52056 Aachen, Germany

[19]Oskar Klein Centre and Dept. of Physics, Stockholm University, SE-10691 Stockholm, Sweden

[20]Physikalisches Institut, Universität Bonn, Nussallee 12, D-53115 Bonn, Germany

[21]Dept. of Physics and Astronomy, Uppsala University, Box 516, S-75120 Uppsala, Sweden

[22]Dept. of Physics, Pennsylvania State University, University Park, PA 16802, USA

[23]Dept. of Physics, TU Dortmund University, D-44221 Dortmund, Germany

[24]Laboratory for High Energy Physics, École Polytechnique Fédérale, CH-1015 Lausanne, Switzerland

[25]Max-Planck-Institut für Kernphysik, D-69177 Heidelberg, Germany

[26]Dept. of Astronomy and Astrophysics, Pennsylvania State University, University Park, PA 16802, USA

[27]Vrije Universiteit Brussel, Dienst ELEM, B-1050 Brussels, Belgium

[28]Dept. of Physics and Astronomy, Utrecht University/SRON, NL-3584 CC Utrecht, The Netherlands

[29]CTSPS, Clark-Atlanta University, Atlanta, GA 30314, USA

[30]Dept. of Physics, Southern University, Baton Rouge, LA 70813, USA

[31]Dept. of Astronomy, University of Wisconsin, Madison, WI 53706, USA

[32]Dept. of Physics, University of Alberta, Edmonton, Alberta, Canada T6G 2G7

[33]Institute of Physics, University of Mainz, Staudinger Weg 7, D-55099 Mainz, Germany

[34]Université de Mons, 7000 Mons, Belgium

[35]Dept. of Physics, Chiba University, Chiba 263-8522, Japan

[36]Institut für Physik, Humboldt-Universität zu Berlin, D-12489 Berlin, Germany

[37]also Sezione INFN, Dipartimento di Fisica, I-70126, Bari, Italy

[38]Dept. of Physics and Astronomy, University of Alaska Anchorage, 3211 Providence Dr., Anchorage, AK 99508, USA

[39]Dept. of Physics, University of the West Indies, Cave Hill Campus, Bridgetown BB11000, Barbados

[40]NASA Goddard Space Flight Center, Greenbelt, MD 20771, USA

[41]School of Physics and Center for Relativistic Astrophysics, Georgia Institute of Tech-

48 Received _____; accepted _____

nology, Atlanta, GA 30332, USA

[42]Dept. of Physics and Astronomy, University of Alabama, Tuscaloosa, AL 35487, USA

ABSTRACT

This paper presents a search for flares of neutrinos that may have not been detected by the time-integrated searches previously performed by the IceCube experiment. For the first time, a search is performed over the entire parameter space of energy, direction and time looking for neutrino flares from astrophysical sources among the atmospheric neutrino and muon backgrounds. Time-integrated searches are less sensitive to flares because they are affected by a larger background of atmospheric neutrinos and muons that can be reduced by the time constrain. Flaring sources considered here, such as Active Galactic Nuclei, Soft Gamma Ray Repeaters and Gamma Ray Bursters, are promising candidate neutrino emitters.

We used mainly data taken between April 5, 2008 and May 20, 2009 by a partially completed configuration of IceCube with 40 strings. For the presented searches an unbinned maximum likelihood method is used with a time-dependent prior to test several different source hypotheses. The so called "untriggered" search covers any possible time-dependent emission from these sources not correlated to any other observation using other astrophysical messengers such as photons. Moreover, a similar time scan is performed for a predefined catalogue of sources that exhibit intense photon flares.

A "triggered" search by multi-wavelength information on flares from blazars and Soft Gamma Ray repeaters is performed using the 40 string data and also the data taken by the previous configuration of 22 strings in operation between May 31, 2007 and April 5, 2008. Flares for which extensive and continuous monitoring is available from Fermi-LAT and SWIFT and flares detected by Imaging Cherenkov Telescopes with shorter time-scale monitoring are considered. The triggered flare corresponding to the highest significance is from the blazar PKS

1502+106. It was seen by Fermi-LAT in gamma-rays and SWIFT in soft X-rays and optical, but not in hard X-rays. The probability after trials that this is due to a fluctuation of the background is 29%. Each of these results are compatible with a fluctuation of the background.

Even if no positive evidence of signal was found, the presented time dependent search is the first one performed on neutrinos that covers the range between 20 μs to a year timescale.

Subject headings: triggered searches, multi-wavelength campaigns, blazars, soft-gamma ray repeaters, micro-quasars

85 ## Contents

1. Introduction

Several astrophysical sources are known to have a variable photon flux at different wavelengths, exhibiting flares. Hadronic models predict neutrino emission associated with photons due to pion photoproduction. These neutrinos are unique messengers to explore the universe because they have no charge and interact weakly. Their detection would be a confirmation that hadronic acceleration is taking place in astrophysical sources.

Time-integrated analyses are less sensitive for flares because they contain a higher background of atmospheric neutrinos and atmospheric muons. Time-dependent analyses reduce this background by searching over smaller time scales around the flares. The searches discussed in this paper are about a factor of four to five more powerful than time-independent searches for flares of ~ 1 sec.

IceCube is a 1 km^3 neutrino telescope located at the South Pole. Its major goal is to discover high energy neutrinos of extraterrestrial origin. Four searches for time-dependent neutrino emissions from various categories of flaring sources are presented in this paper. We call "triggered" searches those using multi-wavelength (MWL) information from photon experiments. Based on this information, we select catalogues of interesting candidate neutrino-emitting flares from sources such as AGNs and SGRs. We use a likelihood ratio method that compares a signal plus background hypothesis and a background only one. The underlying assumption of triggered searches is that the neutrino emission follows the time-dependent properties of the photons, as a consequence of an enhanced state of the source when the jet can accelerate particles to higher energies than in the quiescent state. This hypothesis is assumed in the likelihood method as a prior. In order to make the search

for flare as general as possible, also an "untriggered" scan looking for a clustering of events in time and direction without prior timing information is performed. Untriggered searches are affected by large trial factors, hence reduced catalogues of sources and additional MWL information are used to help enhance the discovery potential.

The paper is divided as follows. In Sec. 2 the properties of the flaring sources are considered, Active Galactic Nuclei (AGNs), gamma-ray bursts (GRBs) and soft-gamma repeaters (SGRs). In Sec. 3 the data sample from 40 strings and 22 strings of IceCube is described. In Sec. 4 the time-dependent likelihood method is illustrated in general and how it compares with the time-independent method. The four searches for flares are:

- An untriggered all-sky scan for short duration point source emission of neutrinos (Sec. 5);
- An untriggered search for flares from a predefined catalogue of 40 sources identified as variable in GeV photons (Sec. 6);
- A triggered search using MWL information for continuously monitored sources. Data from Fermi-LAT and also from SWIFT (Sec. 7) are used.
- A triggered search using sporadic information on flares collected by various X-ray experiments and Imaging Cherenkov Telescopes (IACTs) with typical energy thresholds around 300 GeV (Sec. 8). These experiments have a reduced duty cycle compared to Fermi and tend to monitor sources mainly during their flaring states.

In each section the search method and its expected discovery potential are shown, and results are provided. In all searches the background is estimated directly from data, since the signal contribution is expected to be small. To avoid any bias toward discovery, each search has been performed in a blind fashion by defining cuts and search methods before

looking at the time of the final event sample. The final significance, which accounts for the different trials, is calculated by scrambling data in time. For each search the resulting p-values are provided. The post-trial significance with respect to all searches should account for the fact that four different searches are performed. Since this trial factor is negligible compared to the 5σ significance required by IceCube for a claim of discovery, it is not explicitly added in each search.

2. Candidate Sources of Flaring Neutrino Emission

Galactic and extra-galactic sources exhibit time-dependent emissions that range from short bursts of the order of seconds up to minutes from GRBs or giant flares from SGRs, to longer flares from AGNs, lasting from hours to weeks.

Variable emission from AGNs is one of the main targets of the searches presented in this paper. Flat-Spectrum Radio Quasars (FSRQs) and BL Lacs, commonly unified in the AGN class of blazars, exhibit relativistic jets pointing towards the Earth and some of the most violent variable high energy phenomena. Their spectral energy distributions (SEDs) extends orders of magnitudes across the electromagnetic spectrum and are characterized by a double-peaked structure composed of a thermal and a non thermal component. The Fermi-LAT collaboration recently published their first AGN catalogue (Abdo & Collaboration 2010) after 11 months containing 709 GeV-sources associated to AGNs many of which are in the previously published Bright Source list catalogue (Abdo et al. 2009b). A stacking search for neutrinos from AGNs has been published in the past using AMANDA data (Achterberg et al. 2006c).

The thermal component of the AGN's SED is made of infrared radiation from a warm, dusty torus heated by a central source, and of Optical/UV emission of the accretion disk

due to hot gas. The low energy non-thermal component in the radio to soft X-rays is due to synchrotron radiation of electrons gyrating in a magnetic field. The high energy non-thermal component (X-ray to γ-ray) is explained in leptonic jet models by synchrotron emissions of electrons in the jet and subsequent up-scattering of photons (Inverse Compton) by the same electrons responsible for the synchrotron emission (for a review on all models see e.g. Boettcher (2010, 2007) and references therein). While leptonic models enjoy relatively good success reproducing the observed emission, there are compelling arguments in favor of a hadronic component. If a significant fraction of the jet power is converted into the acceleration of relativistic protons in a strongly magnetized environment, reaching the threshold for p-γ pion production, synchrotron-supported pair cascades will develop and also neutrinos would consequently be produced.

The emission from blazars is known to be variable at all wavelengths. Simultaneous MWL observations are therefore crucial for understanding what phenomena can cause this variability (Gaidos et al. 1996; Blazejowski et al. 2005; Kartaltepe & Balonek 2007; Horan et al. 2009; Boettcher et al. 2009). The intensity of these objects can vary by more than an order of magnitude between different observing epochs. The typical time scales of AGN flares vary between hours to days, though high-energy variability has been observed on much shorter time scales, in some cases even down to just a few minutes (Aharonian 2007; Albert et al. 2007).

Perhaps the most compelling evidence for a hadronic component are observations of "orphan" flares, defined as TeV emissions without accompanying X-rays, such as the 1ES 1959+650 flare in 2002 (Krawczynski et al. 2004). An a posteriori observation with AMANDA-II of two events (Bernardini et al. 2005), one exactly during the flare and another 31 days later, triggered some theoretical calculations (Halzen & Hooper 2005; Reimer et al. 2005). Two recent suspected orphan flares are included in the source catalogs for the MWL

triggered searches (see Sec. 7 and 8).

GRBs, believed to be produced by the most powerful phenomena in the universe (Meszaros 2006; Piran 2004), are interesting candidate flaring neutrino sources ((Waxman 2003; Meszaros & Rees 1993)). IceCube conducts dedicated searches for these objects triggered by satellite information (Abbasi et al. (2010c), Abbasi et al. (2009c), (Abbasi et al. 2010d)). The untriggered all-sky search presented in this paper is also sensitive to this source class if two or more neutrinos can be detected from the same GRB. While the dedicated searches are in general much more sensitive (because they use the known time and direction of GRBs observed in gamma- or X-rays), the untriggered search has the potential to detect a burst which was not observed in photons (due to e.g. absorption or lack of monitoring).

Another possibility for powerful emission is given by SGR's, X-ray pulsars that show variability at different timescales and a persistent X-ray emission with luminosity $L \sim 10^{35}$ erg/s with short bursts of X- and γ-rays with $L \sim 10^{41}$ erg/s lasting $\sim 0.1 - 1$ s (for review see Mereghetti (2008)). These X-ray pulsars, together with Anomalous X-ray Pulsars, are considered to be the best candidates for magnetars, isolated neutron stars powered by huge magnetic fields ($B \sim 10^{15}$ G). At times these sources exhibit "giant" flares with initial spikes of hard non-thermal radiation up to luminosities of $\sim 10^{46}$ erg/s lasting some seconds. These flares saturate most detectors due to the enormous photon fluxes, and may accelerate baryons and produce neutrinos (Halzen et al. 2005; Ioka et al. 2005; Liu et al. 2010). AMANDA-II published neutrino and photon limits from the powerful giant flare observed in Dec. 2004 from SGR 1806-20 (Achterberg et al. 2006b). In the catalogue (Tab. 4) used in one of the triggered flare searches (Sec. 8), a period of intense flares from SGR 0501+4516 discovered by SWIFT on Aug. 22, 2008, and observed also by RXTE, Konus Wind and the Fermi GBM (Kumar et al. 2010) is also considered.

3. The IceCube Detector and the Data Sample for this Analysis

The IceCube Neutrino Observatory is composed of a deep array of 86 strings holding 5,160 digital optical modules (DOMs) instrumented between 1.45 and 2.45 km below the ice surface at the geographic South Pole. IceCube strings are separated by about 125 m with DOMs positioned vertically 17 m apart along each string. Each DOM consists of a Hamamatsu photomultiplier with 25 cm diameter (Abbasi et al. 2010a), electronics for waveform digitization (Abbasi et al. 2009d), and a spherical, pressure-resistant glass housing. IceCube construction started with a first string installed in the 2005-6 season (Achterberg et al. 2006a) and has recently been completed in the austral summer of 2010-11. The configurations of IceCube that have been used for the present analysis (22-string and 40-string) are shown in Fig. 1. The IceCube Neutrino Observatory includes a dense subarray, DeepCore, designed to enhance physics performance of IceCube below 1 TeV and a surface array, IceTop, for extensive air shower measurements on the composition and spectrum of cosmic rays.

Identification of neutrino-induced muon events in IceCube was demonstrated by (Achterberg et al. 2007a) using atmospheric neutrinos as a calibration tool. The measurement of atmospheric neutrinos for the 40-string configuration has been presented in (Abbasi et al. 2010b) . This sample of upgoing events dominated by atmospheric neutrinos is used to look for astrophysical signals from point sources using directional and energy information. Since Abbasi et al. (2009a), the IceCube field of view has been extended to also include downgoing events from southern hemisphere. In this case, the background sample in the downgoing region is made of very high energy muons. Since muons are roughly five orders of magnitude more numerous than atmospheric neutrinos at the depth of IceCube, their number is reduced by selecting high energy events so that the astrophysical signal can potentially emerge, if its spectrum is harder than that of the atmospheric neutrino and

muon background. This results in a different sensitivity for the northern hemisphere, where TeV-PeV neutrino astronomy is possible, with respect to the southern hemisphere, where only PeV-EeV neutrino searches are performed in the current analysis.

The selection of the data from the IceCube 40-string configuration used in this search is discussed in the paper on the time independent searches (see Abbasi et al. (2010e)). We refer to this paper for all details on the selection of the muon events in the filtered stream (L1) that is sent over satellite from the South Pole and on the final cuts to obtain the data sample used in this analysis. The cuts were optimized using an E^{-2} spectrum signal, as it is expected for neutrinos directly accelerated in astrophysical sources compared to the measured softer atmospheric neutrino spectra. We also refer to this paper for a detailed discussion on the analysis method. The final sample consists of 36,900 atmospheric neutrino and muon events from the whole sky (-85° to +85° in declination) detected by IceCube in the 40-string configuration in 375.5 days of good data taking, which corresponds to 92% uptime of the nominal operation period between April 5, 2008 and May 20, 2009 or Modified Julian Day (MJD) 54561-54971. In this sample, 14,121 events are up-going, while 22,779 events are down-going. The systematic errors have been evaluated and presented in Sec. 6 of Ref. Abbasi et al. (2010e) for the 40-string data and have also been discussed in Abbasi et al. (2009b) for the 22-string data. The main uncertainties on the limits to the fluence of an E^{-2} signal of muon neutrinos come from photon propagation, absolute DOM efficiency, and uncertainties in the Earth density profile and muon energy loss, accounting for a total of 16%. In this paper we focus on demonstrating the stability in time of the data selected for this search and on the effects of the detector asymmetry for short signals lasting less than 1 day, showing that this was accounted for the searches presented here.

In the triggered search for flares (Sec. 8) we also consider events during data taking with 22 strings of IceCube, which has a livetime of 275.7 days, or a total livetime of 89%

of the operation period from May 31, 2007 to April 5, 2008 (MJD 54251-54561). The selection of this sample is described in Abbasi et al. (2009b), and consists of 5114 candidate events from declinations -5° to +85°. Deadtime for this analysis is mainly due to test and calibration runs during and after the construction season.

IceCube uses a simple multiplicity trigger, which requires that at least eight DOMs are triggered within 5 μs. For a DOM to trigger, it is both required that the DOM PMT voltage crosses the discriminator threshold (0.25 of a typical photoelectron), and each hit to be in coincidence with at least one other hit in the nearest or next-to-nearest neighboring DOMs within $\pm 1\mu$s. This greately reduces hits due to uncorrelated PMT noise and radioactivity in the glass. Once the detector is triggered, all DOM information within a ± 10 μs window is read out and merged to create an event. This means that 20 μs is the effective limit on how close two events can be in time for the 40-string data.

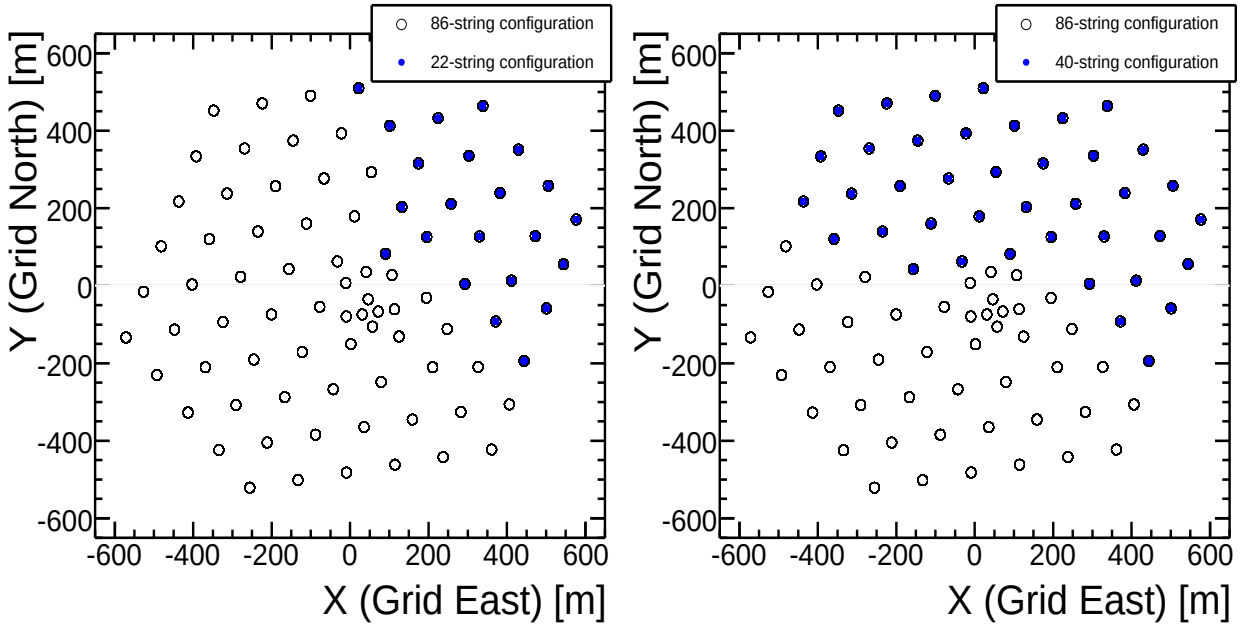

Fig. 1.—: The 22-string (left) and 40-string (right) configurations of IceCube seen from the top. Full circles inside empty circles (corresponding to strings) indicate each configuration.

Standard IceCube runs are eight hours long, with roughly two minutes between the end of one run and the beginning of the next. This run transition time is necessary to stop and restart the DAQ software. The rate of each run is monitored and checked for any deviation from an average that accounts for seasonal fluctuations (Tilav et al. 2009).

The livetime for this analysis is 92.3% during which the detector is stable and operational. For some short periods parts of the detector can be excluded from the acquisition, but still the remaining part can be useful in case an astrophysical event occurs (see e.g. Abbasi et al. (2009c)) All runs used for this analysis had all 40 strings taking data, as well as 22-string data for the analysis presented in Sec. 8.

At low levels of cuts the data sample is dominated by downgoing atmospheric muons. This is the case in the upgoing region as well, since some atmospheric muons are misreconstructed as upgoing and must be rejected in the process of applying analysis cuts. The atmospheric muon rate exhibits a seasonal variation of roughly $\pm 10\%$ due to changes in density of the atmosphere at the South Pole between winter and summer. When the atmosphere is warmer and less dense during the austral summer, the fraction of pions and kaons in air showers which decay before interacting is increased compared to the winter. The muon rate also varies several percent on timescales of few days as a result of weather phenomena in Antarctica. For atmospheric neutrinos detected from the upgoing region, where the Earth acts as a filter for the much larger atmospheric muon flux, the seasonal variations are smaller, approximately 6% (Achterberg et al. 2007b; Abbasi et al. 2010b), since neutrinos are created over a wide range of Earth's latitudes compared to the atmospheric muons created near the South Pole. The rate stability in runs used for analysis was checked, accepting only good quality runs, i.e. with a rate larger or smaller than 5σ from the rolling average (± 2 days) calculated event rate. This loose constrain allows for short-term weather variability. The rate of events, mostly track-like ones, as a function

of time for the 40-string runs is shown in Fig. 2, where the seasonal modulation is clearly visible. For 22 strings the rates of a sample of muon filter data selected with weak cuts is shown in Fig. 3. The rate of the 40 string final event sample is shown in Fig. 4 for upgoing and downgoing events and for the total sample.

Due to the requirements for triggering and filtering, the cuts applied, Earth absorption properties and detector geometry, the final sample of events is not uniform in the detector local coordinates zenith (θ), and azimuth (ϕ). For time-integrated point source searches, the azimuth dependence is usually neglected because it is smoothed in right ascension by the rotation of the Earth over long integration times. However, in a time-dependent analysis the azimuth dependence becomes important for time scales shorter than 1 day. The local coordinate (zenith and azimuth) distribution of 40 string data is shown in Fig. 5 (left). In the northern sky there is an effect that events which travel along the longer end of the detector have a longer lever arm, and are more likely to trigger the detector and be well-reconstructed. In the southern sky, there is an initial cut for online filtering on the integrated charge seen in all DOMs for a given event. This gives a preference to events which pass near a line of strings, yielding a six-fold peak in rates corresponding to the main axes of the detector symmetry.

4. Unbinned Time-Dependent Likelihood Method

The unbinned likelihood searches performed here are based on the methods described in Braun et al. (2008) and specifically applied to time-dependent searches in Braun et al. (2010). In this likelihood ratio method, the data are modeled as a combination of signal and background populations. For a data set with N total events, where n_s is the number of signal events, the probability density of the i^{th} event is given by:

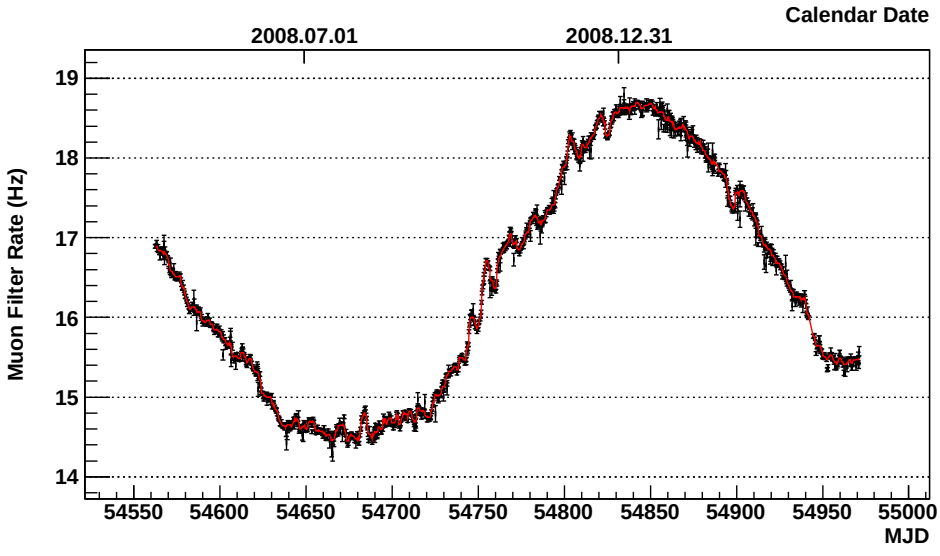

filtered stream

Fig. 2.—: The rate per run of the filtered stream of muon events selected at the South Pole for the 40-strings detector as a function of MJD. The sliding average rate is marked in red and it is calculated over a time interval of ±2 days. The small modulations around the main seasonal oscillation are due to short-term weather variability.

.

$$\frac{n_s}{N}\mathcal{S}_i + (1 - \frac{n_s}{N})\mathcal{B}_i. \tag{1}$$

The likelihood $\mathcal{L}$ of the data given the value of n_s is the product of the individual event probabilities:

$$\mathcal{L}(n_s) = \prod_{i=1}^{N} \Big[\frac{n_s}{N}\mathcal{S}_i + (1 - \frac{n_s}{N})\mathcal{B}_i\Big]. \tag{2}$$

This likelihood is maximized with respect to n_s and any other nuisance parameters which are a part of the signal hypothesis. The maximization provides the best-fit values of these parameters. The background probability distribution function, or pdf, B_i, is given by:

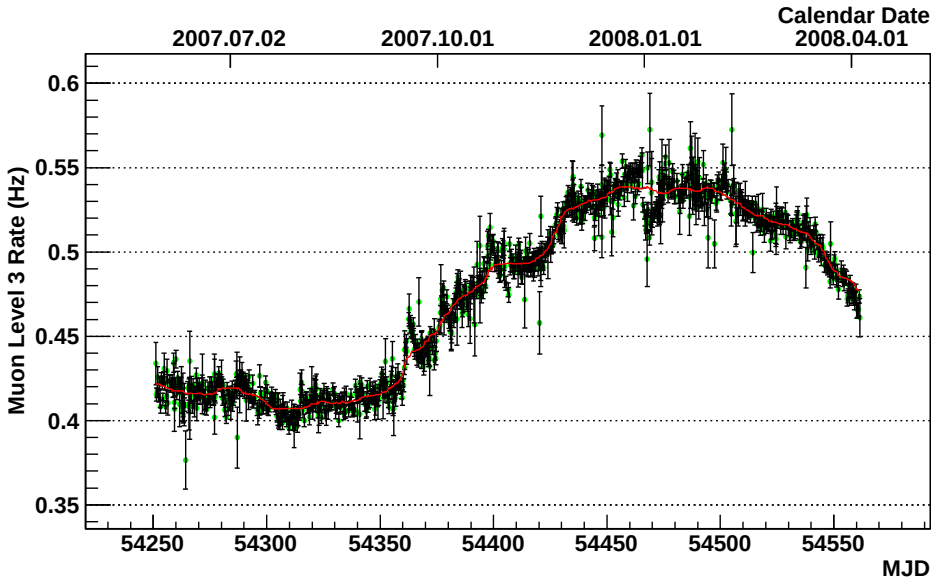

Fig. 3.—: Same as Fig. 2 but for this plot, since the filtering scheme for the 22-string data differed compared to the 40-string data, only upgoing events are selected. The upward going events at these level of cuts are still dominated by atmospheric muons and not by neutrinos, hence seasonal variations are clearly visible.

$$B_i = B_i^{space}(\theta_i, \phi_i) B_i^{energy}(E_i, \theta_i) B_i^{time}(t_i, \theta_i), \tag{3}$$

and is computed using the distribution of data itself.

The spatial term $B_i^{space}(\theta_i, \phi_i)$ is the event density per unit solid angle as a function of the local coordinates, shown in Fig. 5 (left). The energy probability, $B_i^{energy}(E_i, \theta_i)$, is determined from the energy proxy distribution of data as a function of the cosine of the zenith angle $\cos\theta_i$ (see Fig. 5 on the right). This energy proxy, described in detail in Abbasi et al. (2010e), uses the density of photons along the muon track due to stochastic energy losses of pair production, bremsstrahlung and photonuclear interactions which dominate over ionization losses for muons above 1 TeV. The energy cut for the southern sky sample decreases for larger zenith angles, creating a strong zenith dependence of the energy in the

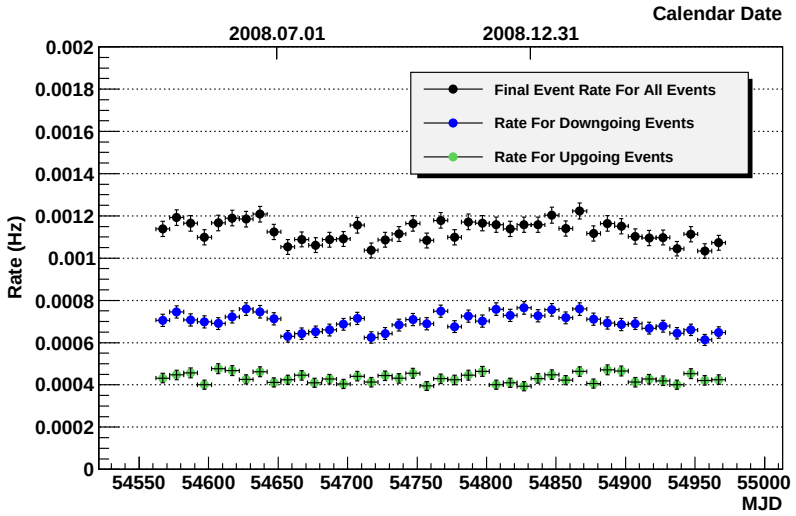

Fig. 4.—: A plot of the rate of events at final level, in bins of 10 days. Errors are statistical. Also plotted are the individual rates of upgoing and downgoing events. The total fluctuation in the final data rate is $\pm 5\%$ for downgoing events and $\pm \sim 4\%$ for upgoing events. The analysis in Sec. 6 uses a sinusoidal fit to the atmospheric muon event rate to estimate rate fluctuations in the downgoing region. All other searches neglect these event rate fluctuations, which are negligible compared to statistical fluctuations in the expected signal.

southern sky as can be seen in Fig. 5 (right). Note that for the northern sky the energy dependence on zenith is small. The time probability $B_i^{time}(t_i, \theta_i)$ of the background can be taken to be flat since the expected seasonal modulations are less than $\pm 10\%$, which is negligible compared to possible signal fluctuations, or use information on an expected seasonal modulation. The magnitude of the seasonal modulation also depends on the zenith angle.

The signal pdf S_i is given by:

$$S_i = S_i^{space}(\mid \vec{x}_i - \vec{x}_s \mid, \sigma_i) S_i^{energy}(E_i, \theta_i, \gamma_s) S_i^{time} \quad , \tag{4}$$

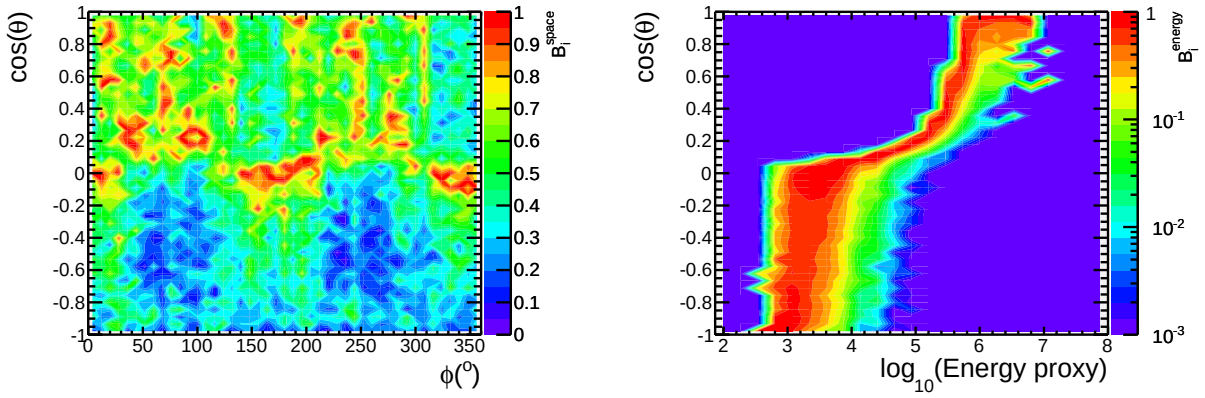

Fig. 5.—: Left: The spatial term in eq. 3: the normalized final event distribution in local coordinates for the 40 strings data (the space term in eq. 3). There are two predominant effects in the local coordinates distribution: for upgoing events (northern sky, bottom half), events traveling down the longer end of the detector are more likely to trigger and pass cuts; for downgoing events (southern sky, top half), there are six peaks in the event rate. This is due to the initial filter conditions at the South Pole that selects tracks more efficiently when they pass close to aligned strings. Right: The energy term in eq. 3: normalized distribution of sine of the declination as a function of the energy proxy.

where S_i^{space} depends on the angular uncertainty of the event σ_i and the angular difference between the event coordinate $\vec{x}_i$ from the source coordinate $\vec{x}_s$. S_i^{energy} is a function of the reconstructed energy proxy E_i, and the spectrum γ_s is calculated from an energy distribution of simulated signal in a zenith band that contains the event. S_i^{time}, the signal time probability, depends on the particular signal hypothesis, which will be different in each search described in this paper.

The test statistic (TS) is calculated from the likelihood ratio of the background-only (null) hypothesis over the signal-plus-background hypothesis:

$$TS = -2\log\Big[\frac{\mathcal{L}(n_s = 0)}{\mathcal{L}(\hat{n}_s, \hat{\gamma}_s, \hat{T}_s)}\Big]. \tag{5}$$

The test statistic is expressed as in eq. 5 to have it distribute as a chi-square function with number of degrees of freedom equal to the fit parameters. By maximizing the likelihood ratio the best fit parameters $\hat{n}_s, \hat{\gamma}_s$ and the time parameters $\hat{T}_s$ are obtained. Larger values of TS are less compatible with the null hypothesis, and indicate its rejection at a confidence level equal to the fraction of the scrambled trials above the TS value found in the data. The data is scrambled by assigning a random time to each event tracking the detector uptime (i.e. either on or off) and performing the same coordinate transformation to get to scrambled right ascension.

The fraction of trials above the TS value obtained from data is referred to as the *p-value*, with smaller values indicating that the background-only (i.e. null) hypothesis is increasingly disfavored compared to the signal-plus-background hypothesis as a description of the data. This leads to the definition of the discovery potential: the average number of signal events required to achieve a p-value less than $2.87{\times}10^{-7}$ (one-sided 5σ) in 50% of trials. Similarly the sensitivity is defined as the average signal required to obtain a p-value less than that of the median test statistic of scrambled samples in 90% of trials.

Aside from presenting the p-values from searches, in the absence of a signal upper limits on the fluence are provided, defined as the integral in energy and time of the flux upper limit:

$$f = \int_{t_{min}}^{t_{max}} dt \int_{E_{min}}^{E_{max}} dE{\times}E\frac{dN}{dE} = \Delta t \int_{E_{min}}^{E_{max}} dE{\times}E\left(\Phi_0 E^{-2}\right) = \Delta t \Phi_0 \left[\ln(E_{max}) - \ln(E_{min})\right] \ , \tag{6}$$

where Φ_0 is the upper limit on the normalization on an E^{-2} spectrum and E_{min} and E_{max} are the central 90% containment bounds of the neutrino energies obtained from simulation and dependent on declination. Δt is the duration of the emission. There is a correspondence

between the fluence and the average number of events detected, shown as a function of the declination in Fig. 6. The limits are calculated according to the Neyman-Pearson lemma (Neyman & Pearson 1933) and the systematic error of 16% is neglected in all upper limits since the limits are dominated by statistical fluctuations for flares.

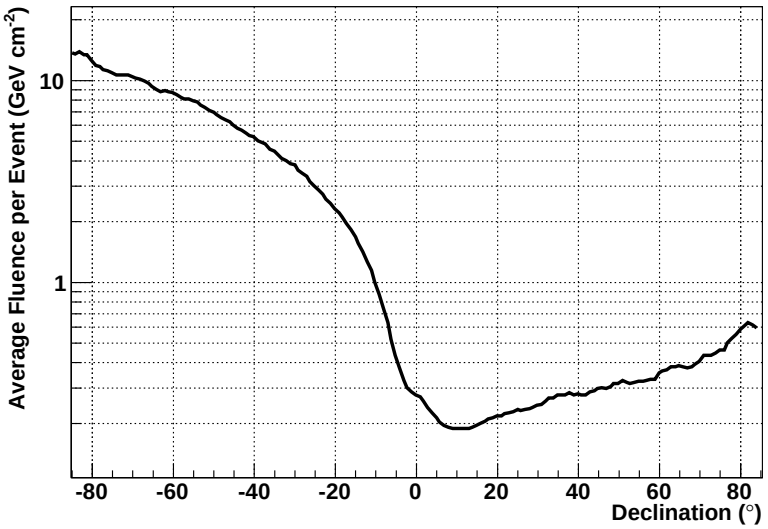

Fig. 6.—: The total fluence from events in a declination band divided by the number of events from an E^{-2} muon neutrino signal in the 40-string configuration, plotted against declination.

5. All-Sky Time-scan

The all-sky time-dependent search presented here complements the all-sky search applied to the IceCube 40-string data in (Abbasi et al. 2010e). While that search has the best sensitivity to steady sources, a source which has emitted neutrinos for only a limited period of time might skip detection. The time-dependent analysis here scans for a significant excess with respect to background over all time scales (from sub-seconds to the full year) at each direction of the sky. For flares shorter than ∼100 days, the discovery

potential of the time-dependent search typically becomes better than the time-integrated one, and in principle a short burst can be discovered with only two events if they occur close enough together in time. The advantage of such untriggered searches is to cover all possible options, including neutrino emission occurring while no photon experiment observes connected emissions.

5.1. Method and Expected Performance

The method in Braun et al. (2010) is adapted for this search to a real detector with non-uniform acceptance and deadtime. The time dependent probability density function from eq. 4 for this search is a Gaussian function:

$$S_i^{time} = \frac{1}{\sqrt{2\pi}\sigma_T} \exp\left(-\frac{(t_i - \mathrm{T}_\circ)^2}{2\sigma_T^2}\right) \tag{7}$$

where t_i is the arrival time of the event, and $\mathrm{T}_\circ$ and σ_T are the mean and sigma of the Gaussian describing flaring behavior in time. The maximization of the test statistic returns the best-fit values of the Gaussian mean (the time at which the flare peaks) and sigma (corresponding to the duration of the flare). Since the number of events expected from a flare is small, the statistics limit the sensitivity to a specific function.

Because there are many more independent small time windows than large ones, the test statistic formula of eq. 5 is modified to include a marginalization term to correct for this effective trial factor and avoid undue preference for short flares Braun et al. (2010). The test statistic formula that is maximized is then:

$$TS = -2\log\left[\frac{\mathrm{T}}{\sqrt{2\pi}\hat{\sigma}_T} \times \frac{\mathcal{L}(n_s = 0)}{\mathcal{L}(\hat{n}_s, \hat{\gamma}, \hat{\sigma}_T, \hat{\mathrm{T}}_\circ)}\right], \tag{8}$$

where the first factor in the square brackets is the marginalization term and the second

is the likelihood ratio. T is the total livetime of data taking, $\hat{n}_s, \hat{\gamma}, \hat{\sigma}_T, \hat{\mathrm{T}}_\circ$ are the best-fit values for the number of signal events, spectral index, width and mean of the Gaussian flare, respectively. In order to prevent the marginalization term from becoming less than 1 an upper limit is placed on the flare width σ_T. This is done to prevent flares with zero amplitude ($\hat{n}_s$=0) from having a positive test statistic, which would happen if the flare width σ_T were allowed to be greater than $\frac{\mathrm{T}}{\sqrt{2\pi}}$.

As described in Braun et al. (2010), the numerical maximizer needs an initial candidate flare (a "seed"). In that paper this seed is obtained by scanning over sets of m temporally consecutive events, where $2 \leq m \leq 5$, testing the sets for compatibility with a flare with an E^{-2} spectrum. The best candidate is used as the initial seed in the likelihood maximization. In the current analysis, the maximum number of consecutive scanned events has been increased to m = 10 to improve the sensitivity to longer flares. This brings the performance of the analysis close to that of the corresponding time-independent analysis at large time scales. Given that more than 5 events are required for discovery for $\sigma_T > 2$ days (see Fig 7), if the maximum is not increased the method will occasionally only find a subset of the injected events, hence increasing the total signal required to cross the threshold for discovery.

Fig. 7 (left) shows the mean number of events needed for a 5σ discovery for 50% of scrambled samples (black solid line) as a function of the duration of the flare σ_T for a fixed source location at declination of +16°. This is compared to the number of events needed in a time-independent search (black dashed line): the number of events needed to discover a flare of 1s duration is about a factor of 4 lower than for a time independent search. At long timescales the flare search performs only 10% worse than the time-independent search, even with 2 additional free parameters in the fit. In the same plot the median upper limits at 90% c.l. are shown for the time-dependent search and for the time-independent one. On

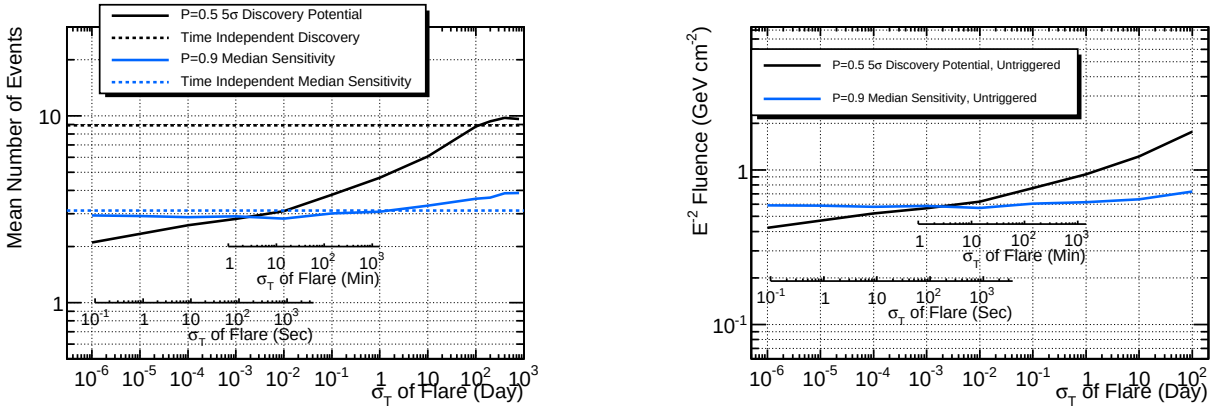

Fig. 7.—: The 50% 5σ discovery potential and 90% median sensitivity in terms of the mean number of events (left) and fluence (right) for a fixed source at $+16^o$ declination. The number of events for the median sensitivity and discovery potential for the time-independent search are also shown. Flares with a σ_T of less than 100 days, or a FWHM of less than roughly half the total livetime, have a better discovery potential than the steady search.

the right the corresponding fluence is given, where a correction is introduced for the median dead time during a given flare as a function of the flare width (see Fig. 8).

The fact that the 5σ discovery potential curve descends below the 90% median upper limit curve is due to the effect of Poisson statistics for the small number of signal events involved. The untriggered search must observe at least two events in order to identify a flare. For a simulated flaring source which injects a mean number of events μ, μ must equal at least 1.68 for 50% of simulated trials corresponding to 2 or more signal events, while μ must equal 3.89 for 90% of the simulated trials for 2 or more signal events. Therefore, at the shortest timescales, the mean signal needed for a discovery in 50% of trials asymptotically approaches 1.68 events, while the mean signal that can be excluded in 90% of trials approaches 3.89 events. The median upper limit 50% of trials with zero and one signal event will have a p-value less than the median, so it saturates at a lower value than 3.89.

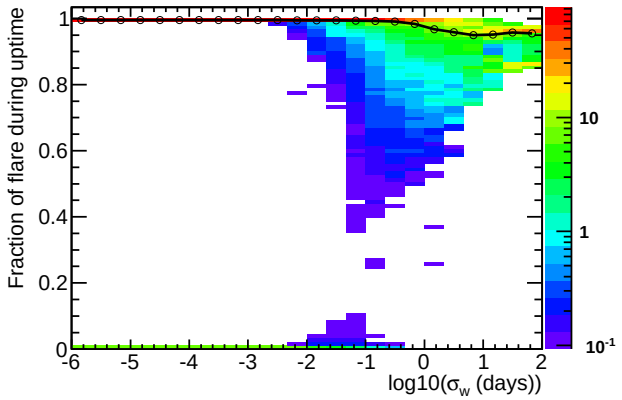

Fig. 8.—: The fractional duration of randomly-simulated flares which occur during the uptime for the 40-string configuration for a range of different flare durations. The black line marks the median fraction of fluence ocurring during the detector livetime for a given flare duration. For instance, for flares shorter than one minute, there is approximately an 8% chance of the flare occuring completely during detector downtime. Flares longer than one day will always have some emission during uptime; on average 92% of the total emission will coincide with usable run time.

The sensitivity saturates at 2.9 events. This is the reason why the discovery potential curve is lower than the sensitivity in Fig. 7.

The method is applied as an all-sky scan over a grid ($0.5^\circ \times 0.5^\circ$) in right ascension and declination. The final result of the analysis is the set of best fit parameters from the location with the highest test statistic value. A final p-value for this analysis is obtained by performing the same scan on scrambled data sets, and counting the fraction of scrambled sets which have a maximum test statistic greater than or equal to the maximum one found for the data.

5.2. Results

Using the 40-string data, the location which deviates most from the background expectation is found at (RA,Dec)=(254.75°, +36.25°). Two events are found, with a best-fit spectrum $\hat{\gamma}$ of 2.15, mean of the flare $\hat{T}_o$ of MJD 54874.7 and width $\hat{\sigma_T}$ of 15 seconds. The two events are 2.0° apart in space and 22 seconds apart in time. The $-log_{10}$(p-value) corresponding to this observation is 4.67. A clustering of higher significance is seen in 56% of scrambled skymaps (see Fig. 9), so this result is consistent with the null hypothesis of background-only data. A large effective trial factor of 2.6×10^4 is generated by scanning the whole sky. Therefore it is desirable to look only at a few sources in order to decrease the trials, which is done in Sec. 6.

Figures 10 to 12 show maps of the pre-trial p-values and best-fit parameters $\hat{T}_o$ and $\hat{\sigma_T}$. It should be noted that the algorithm tends to find shorter flares identifying clusters of events in time over more extended regions than for longer flares (see Fig. 12). This is the result of using two Gaussians to describe each event's angular uncertainty and the flare in time. The test statistic depends on $1/\sigma_T$ (see eq. 8), so this allows their identification over a large area around the flare maximum significance location.

6. Time-scan for Candidate Sources

By targeting specific, a priori promising directions in the sky, an analysis can reduce the effective trial factor of the all-sky scan and therefore improve the discovery potential. One way this can be done is by performing the analysis in Sec. 5 at the specified locations only. Here, this search was instead implemented using a time-clustering algorithm developed in (Satalecka et al. 2007) and (Bazo-Alba et al. 2009), which achieves similar performance. The algorithm finds the most significant flare in a period by testing the most promising

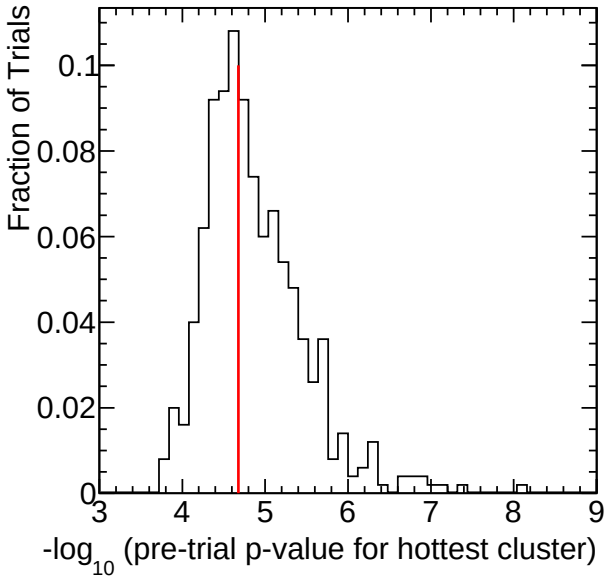

Fig. 9.—: The distribution of the maximum test statistic for the all-sky scan performed on scrambled data sets. Here, the test statistic were first converted to (pre-trial) p-values, so -log(p) is plotted. The value of data is shown in red. 281 out of 500 scrambled skymaps have a more significant flare than that found in the data, so the final p-value of the analysis is 56%.

time windows, which are defined by the times of the neutrino events.

For the source list, variable bright astrophysical objects from the entire sky are selected. Sources are taken from the Fermi-LAT Bright Source List (Abdo et al. 2009b), whose data taking period overlaps with the IceCube 40-string sample. The sources include 30 blazars (24 FSRQs and 6 BL Lacs), one high-mass X-ray binary, one radio galaxy and 7 unidentified objects. In this analysis the following selection criteria are defined for choosing the most promising variable astrophysical sources:

- Classified as variable by Fermi-LAT,

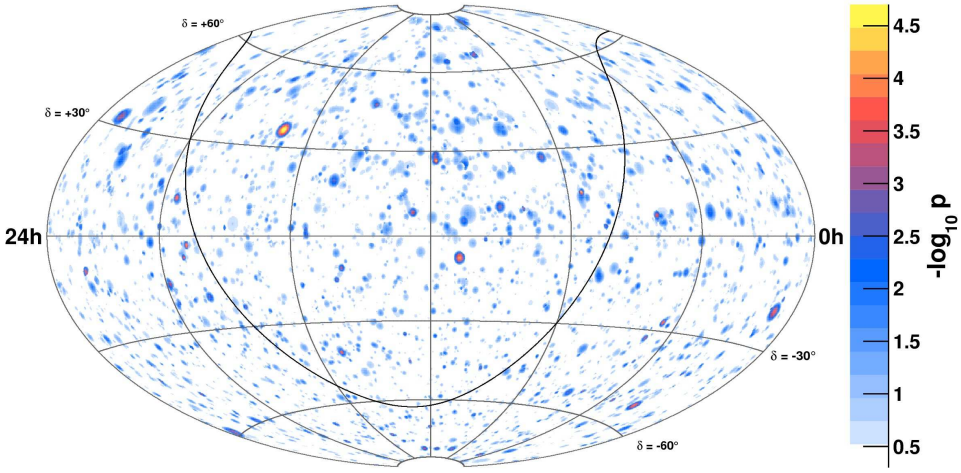

Fig. 10.—: The equatorial coordinate map shows the p-value of the most significant flare in time and space at each location of the grid where the likelihood is calculated. The p-value is indicated on the z-scale on the right. The black curve is the galactic plane.

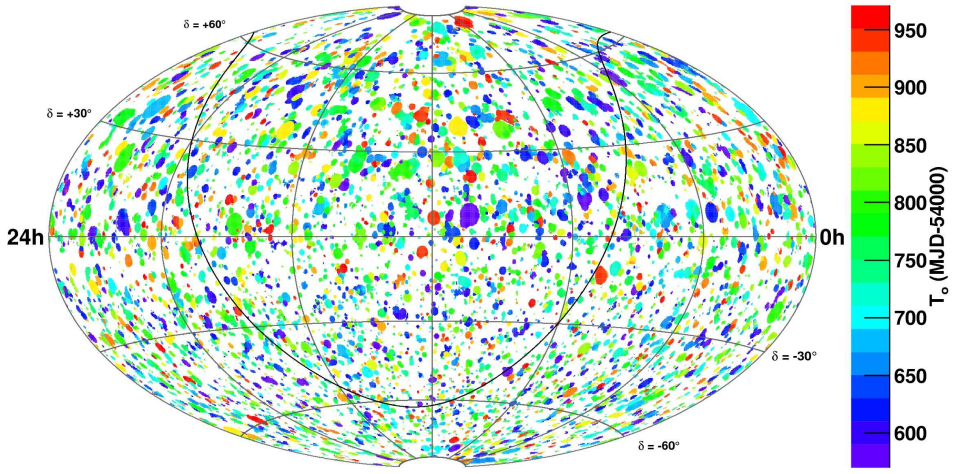

Fig. 11.—: The equatorial coordinate map shows the best fit of the mean time of the flare $\hat{T}_o$ (MJD-54,000) for the most significant flare found at each location of the grid where the likelihood is calculated. The black curve is the galactic plane.

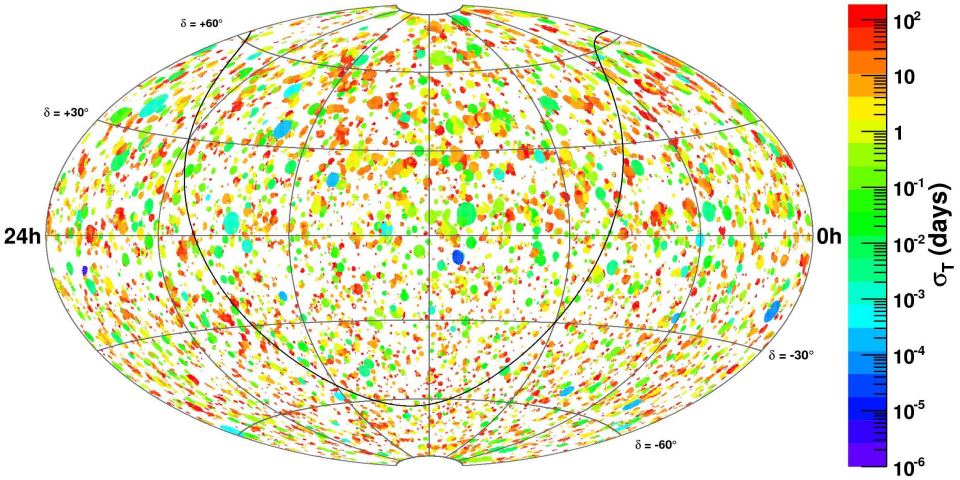

Fig. 12.—: The map in equatorial coordinates of the best fit width $\hat{\sigma_T}$ of most significant flare at a given location found in the search, in days. The black curve is the galactic plane.

- Flux [100 MeV - 1 GeV] $> 1.1 \times 10^{-7}$ photons cm^{-2}s^{-1}.

The definition of variable provided by the Fermi-LAT Bright Source list is that the measured variable emission has only a 1% of being due to a steady source (i.e. variability flag=T). The second requirement sets a minimum photon flux, motivated by the correlation between neutrinos and photons emitted from the source predicted by hadronic models. The average photon flux of all Fermi variable sources is 2.3 $\times 10^{-7}$ photons cm^{-2}s^{-1}. The flux threshold chosen keeps 60% of these sources. The selected candidate list consists of 40 objects (see Table 1), 18 in the southern sky and 22 in the northern sky.

6.1. Method and Expected Performance

For a given source location, signal-like events are defined as having a time-independent $\frac{S_i}{B_i} > 1$, where S_i and B_i are defined in Sec. 4, omitting the time term. Each pair of these event times assigns a starting and ending time (t_i and t_j, respectively), of the flare search

windows $\Delta T_{ij} = t_j - t_i$. The longest flare duration is constrained in the algorithm to be less than 30 days. Apart from this constraint the algorithm loops over all events, testing all windows defined by each set of signal-like events specified above. The test statistic is calculated for the most promising flare time windows and the best time window (i.e. the highest test statistic value) is chosen as a flare candidate.

The signal time probability S^{time} is defined by:

$$S_i^{time}(t_i, t_j) = \frac{1}{\Delta T_{ij}} \quad . \tag{9}$$

The time probability S_i^{time} is constant since no flare time structure is assumed. The statistics of signals expected will be small enough that no particular functional form should be discernable.

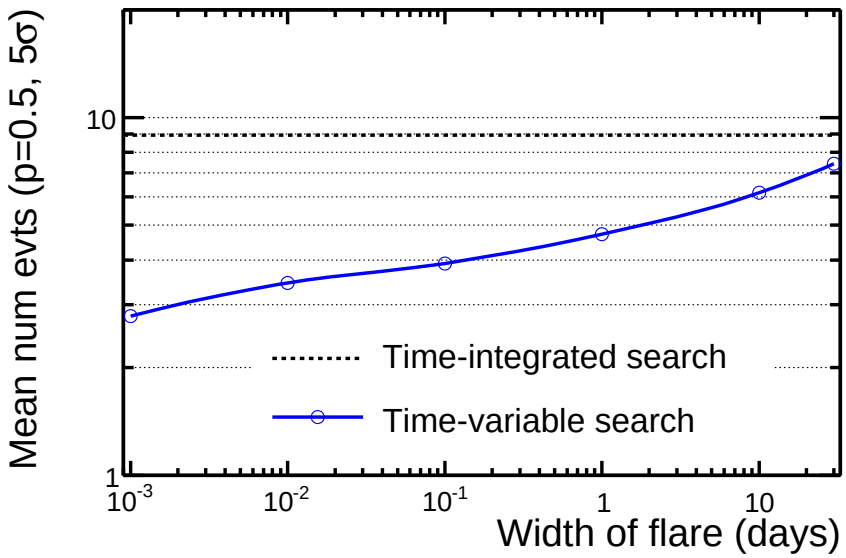

Fig. 13.—: Mean number events for a 5σ discovery in 50% of trials as a function of the flare duration, calculated as an example for a point source at dec=16^o ra=343^o.

The mean number of events needed for this analysis to achieve a 5σ discovery with 50% of trials is calculated for different widths of simulated flares (see Fig. 13). The flare

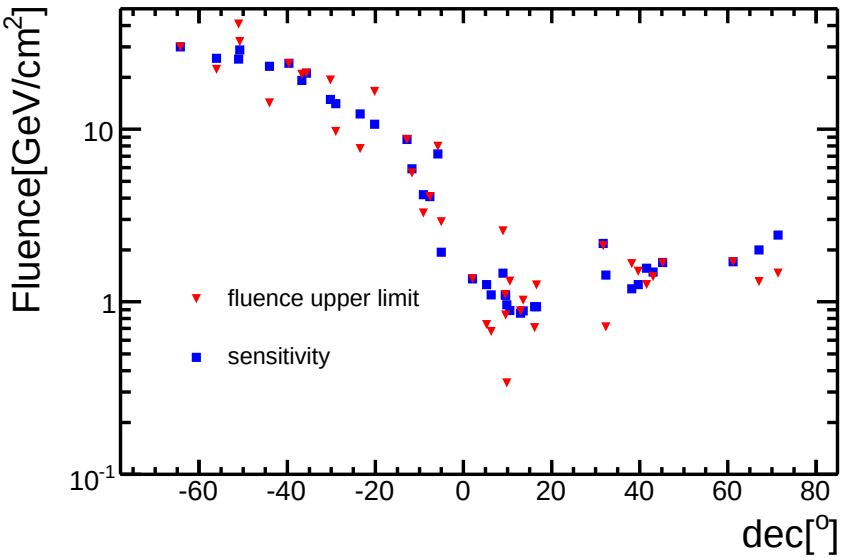

Fig. 14.—: Fluence upper limits (red triangles) of the most significant cluster for each of the 40 selected sources calculated in the time windows given in Tab. 1 versus declination. The blue squares represent the median sensitivity on the fluence calculated for the same time windows.

duration is investigated in the range from 30 days to the minimum time between signal-like events. The discovery potential is very similar to that shown in Fig. 7. For a flare of the order of minutes, one third of the events needed in a time integrated search is necessary for a detection with the untriggered flare method.

6.2. Results

The time-scan looking for neutrino flares was applied to the 40 selected source candidates using IceCube 40-string data. No significant excess above the atmospheric background is found. The results and upper limits for each source are presented in Table 1 and summarized in Fig. 14. The highest fluctuation observed corresponds to

0FGL J0643.2+0858 (dec=8.9^o, ra=100.8^o) with a p-value=7% (1.5 σ) pre-trial. The corresponding best time cluster was 14.3 days, lasting from MJD 54846.5 to 54860.8. Correcting for the trial factor from looking at 40 sources, the final post-trial p-value is 94.9%. The trial factor was calculated by simulating scrambled analyses and applying the search method to the 40 selected directions. The post-trial p-value is obtained from the distribution of the maximum test statistic for many equivalent samples obtained scrambling the time of events.

Table 1:: Results for pre-defined variable astrophysical source candidates using the likelihood time clustering algorithm.

Source (0FGL)	Other Name	dec [°]	ra [°]	$\log E_{min}$ (GeV)	$\log E_{max}$ (GeV)	p-value	Δt (days)	Tstart (MJD)	Fluence Limit (GeV/cm^2)
J1123.0-6416		-64.27	170.8	5.73	7.77	0.89	4.7	54718.1	30.1
J1328.8-5604		-56.08	202.2	5.73	7.78	0.59	0.66	54641.2	22.2
J0210.8-5100	PKS 0208-512	-51.01	32.71	5.72	7.78	0.11	12.9	54750.1	40.6
J0910.2-5044		-50.74	137.6	5.71	7.78	0.38	1.53	54585.7	32.2
J0538.8-4403	PKS 0537-441	-44.06	84.72	5.7	7.8	0.75	3	54833.7	14.2
J1802.6-3939		-39.66	270.7	5.7	7.82	0.97	16.4	54576.3	24.1
J0229.5-3640	PKS 0227-369	-36.68	37.38	5.65	7.82	0.42	4.15	54798.4	20.8
J1457.6-3538	PKS 1454-354	-35.64	224.4	5.64	7.82	0.96	7.17	54788.9	21.2
J2158.8-3014	PKS 2155-304	-30.24	329.7	5.58	7.84	0.15	0.124	54620.6	19.3
J1746.0-2900		-29	266.5	5.58	7.85	0.71	10.4	54934.3	9.69
J0457.1-2325	PKS 0454-234	-23.43	74.29	5.49	7.87	0.72	7	54890.1	7.73
J1911.2-2011	PKS 1908-201	-20.19	287.8	5.42	7.87	0.1	6.45	54696.1	16.6
J1813.5-1248		-12.8	273.4	5.17	7.87	0.5	4.34	54899.7	8.72
J0730.4-1142	PKS 0727-11	-11.71	112.6	5.08	7.86	0.53	0.882	54866.6	5.59
J1512.7-0905	BZQ J1512-0905	-9.093	228.2	4.82	7.79	0.65	13	54855.9	3.27
J2025.6-0736	PKS 2022-07	-7.611	306.4	4.55	7.74	0.91	2.08	54622.6	4.07

Table 1 – continued from previous page

Source (0FGL)	Other Name	dec [°]	ra [°]	$\log E_{min}$ (GeV)	$\log E_{max}$ (GeV)	p-value	Δt (days)	Tstart (MJD)	Fluence Limit (GeV/cm^2)
J1256.1-0547	3C 279	-5.8	194	4.18	7.63	0.45	21.8	54944.4	7.95
J0017.4-0503		-5.054	4.358	4.04	7.59	0.16	3.25	54734.9	2.91
J1229.1+0202	3C 273	2.045	187.3	3.72	7.27	0.96	28.5	54562.7	1.36
J1015.9+0515	PMN J1016+0512	5.254	154	3.73	7.02	0.74	4.46	54915.7	0.74
J1830.3+0617		6.287	277.6	3.72	6.92	0.71	26.2	54624.3	0.675
J0643.2+0858		8.983	100.8	3.7	6.68	0.07	14.3	54846.5	2.57
J2147.1+0931	PKS 2144+092	9.519	326.8	3.69	6.63	0.49	27.8	54737.9	1.1
J1751.5+0935	OT 081	9.591	267.9	3.69	6.63	0.66	6.22	54917.2	0.84
J2327.3+0947	PKS 2325+093	9.794	351.8	3.69	6.62	0.82	2.84	54603.2	0.339
J1504.4+1030	PKS 1502+106	10.51	226.1	3.68	6.58	0.17	6.47	54777.4	1.32
J1553.4+1255	PKS 1551+130	12.92	238.4	3.65	6.46	0.48	0.488	54566.3	0.885
J0531.0+1331	PKS 0528+134	13.53	82.76	3.63	6.43	0.38	0.581	54597	1.02
J2254.0+1609	3C 454.3	16.15	343.5	3.58	6.34	0.66	7.94	54594.4	0.71
J0238.6+1636	AO 0235+164	16.61	39.66	3.57	6.32	0.12	0.216	54776.6	1.25
J1522.2+3143	TXS 1520+319	31.73	230.6	3.38	5.94	0.52	3.95	54869	2.11
J1310.6+3220	B2 1308+32	32.34	197.7	3.37	5.93	0.76	27.7	54671.8	0.716
J1635.2+3809	4C +38.41	38.16	248.8	3.32	5.8	0.092	0.268	54795	1.66

Table 1 – continued from previous page

Source (0FGL)	Other Name	dec [°]	ra [°]	$\log E_{min}$ (GeV)	$\log E_{max}$ (GeV)	p-value	Δt (days)	Tstart (MJD)	Fluence Limit (GeV/cm^2)
J1641.4+3939		39.67	250.4	3.32	5.78	0.29	0.268	54795	1.5
J0320.0+4131	NGC 1275	41.52	50	3.3	5.75	0.62	28.3	54576.7	1.26
J0222.6+4302	3C 66A	43.04	35.65	3.28	5.73	0.51	19.6	54641.1	1.4
J0654.3+4513	B3 0650+453	45.22	103.6	3.25	5.7	0.93	5.85	54903.5	1.69
J0240.3+6113		61.23	40.09	3.1	5.46	0.91	6.19	54699.5	1.71
J1849.4+6706	S4 1849+67	67.1	282.4	3.05	5.28	0.7	10.6	54708.9	1.31
J0722.0+7120	S5 0716+71	71.35	110.5	3.04	5.25	0.75	7.11	54864.7	1.47

Note.- The source name is the 0FGL catalogue designation. The p-value was calculated from simulated background skymaps, Δt is the flare duration of the best cluster and Tstart its starting time. The fluence upper limit was calculated by integrating $d\Phi/dE \times E$ over the 90% energy range and Δt, assuming a neutrino energy spectrum of E^{-2}.

7. Triggered Searches Based on Continuous Photon Observations

When there is specific timing information about the activity of an astronomical object, that information can be used to perform a targeted search with reduced background. This section describes searches in which the photon observations are essentially continuous, and this complete set of flux measurements in time is used. For flares of duration of the order of one second, MWL information can produce a discovery with about a factor of two less signal events with respect to untriggered searches (Braun et al. (2010)).

The source selection was motivated by Fermi alerts, which are only issued for sources seen at a flux level greater than 2×10^{-6} photons/s/cm^2. The selected sources are listed in Tab. 2. These sources include 6 FSRQs, one BL Lac and one unidentified object. The lightcurves were made using the Fermi Public Release data, using the diffuse class event selection. For each source the *Fermi* Science Tools v9r15p2 package is used to select photons from within 2° of each source and calculate the total exposure. Photon events with zenith angles greater than 105° were excluded to avoid contamination due to the Earth's albedo. Time bins of one day width were then used to calculate an average flux. There are two modifications to this procedure: the blazar 3C 454.3 was seen in a massive outburst before official science operation (Abdo et al. 2009a), for this source the published lightcurve from that paper is taken and from the Monitored Source List thereafter. Also, the source PKS 1502+106 was noted to have a large outburst immediately before official science operations began, extending several days after the public information begins (Ciprini 2008; Ciprini et al. 2010). PKS 1502+106 is taken to be flaring since the time of the alert at a fixed flux level. This flaring activity is a possible "orphan flare", because during this period SWIFT observed only soft-gammas and optical emission but not a clear flare in the BAT (15-50 keV).

7.1. Method and Expected Performance

A Maximum Likelihood Block (MLB) algorithm (Scargle 1998; Resconi et al. 2009) is used to "denoise" the lightcurves by iterating over the data points to select periods from the lightcurves which are consistent with constant flux once statistical errors are taken into account. The MLB requires the definition of a confidence level associated with a change of state. For a wide range of values of this parameter, the MLB performs similarly. With the hypothesis that the intensity of the neutrino emission follows the intensity of the photon lightcurve, the signal time pdf is simply the normalized lightcurve itself. A slightly modified hypothesis is that the neutrino emission follows the lightcurve, but only when the photon flux goes above a certain threshold F_{th}. In this case, the value of F_{th} can be used as a free parameter in the analysis, finding the value of the threshold which maximizes the significance of the data. This method also avoids any penalty from making an incorrect *a* priori choice on a flaring threshold. $F(t_i)$ is defined as the value of the denoised lightcurve at t_i and F_{th} is the flux threshold below which no neutrino emission is assumed (i.e. S_i^{time}=0 if $F(t_i) \leq F_{th}$). In the case of $F(t_i) \geq F_{th}$, the probability of neutrino emission is assumed to be proportional to the flux level above that threshold:

$$\rightarrow S_i^{time} = \frac{(F(t_i) - F_{th})}{N_f}; \tag{10}$$

where the normalization factor N_f is the integral of the denoised lightcurve above the threshold. This time dependent pdf is then used as before in eq. 4. This method is illustrated in Fig. 15.

The effect of adding this additional degree of freedom in the fit can be seen in Fig. 16. The effect is small compared to the penalty of fixing the threshold to an incorrect value. The neutrino flux is proportional to the GeV photon flux above some threshold, which is left as a free parameter in the analysis. The effect of allowing an unknown lag between the

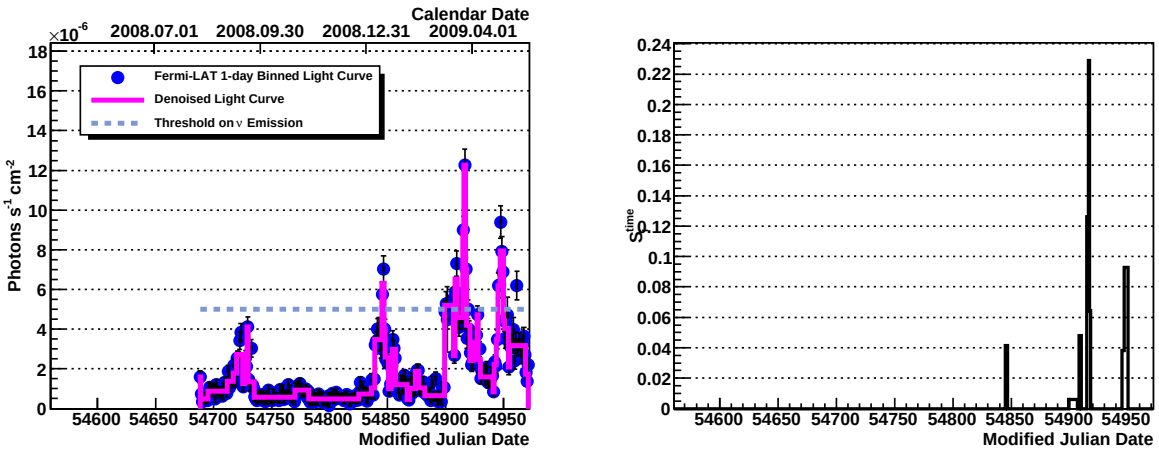

Fig. 15.—: (Left) An example of the one-day binned Fermi lightcurve (blue points, with statistical errors) and denoised lightcurve (pink line) for the blazar PKS 1510-089. The dashed line is an example fit threshold. The lightcurve begins here on August 10, 2008 (MJD 54688), when Fermi science operations began, while the time axis shows the entire 40-string data taking period. (Right) The time pdf used in the neutrino signal hypothesis corresponding to the example photon threshold shown in the left graph (5×10^{-6} photons/s/cm^2).

photon and neutrino emissions was also tested, finding that there was a marked increase in the number of events required for discovery. Hence, we used the method allowing only up to a ± 0.5 day lag that accounts for the 1 day binning of lightcurves.

7.2. Results

The results from all sources are listed in Tab. 2. The most significant source is PKS 1502+106, which has a pre-trial p-value of 5%. The method finds one high-energy event during the August 2008 flare. The prescription to provide the post-trial p-value was to consider the most significant triggered flare between the flares considered with the

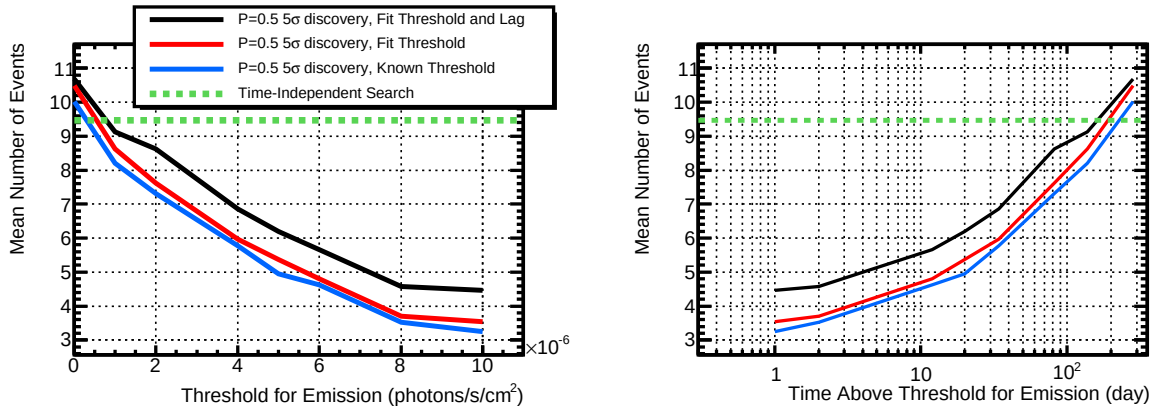

Fig. 16.—: The plot of the 5σ 50% discovery potential for the source PKS 1510-089 (the corresponding lightcurve is shown in Fig. 15), as a function of the true flux threshold for neutrino emission (left) and as a function of the duration the lightcurve spends above the threshold (right). The discovery potential curves are plotted for the time-independent case (dashed line), and from bottom to top for the case where the threshold is fixed to the true threshold (blue line), the case where the threshold is a free parameter (red, used in this analysis) and the case where there is an unknown lag (up to ± 50 days) between GeV and neutrino emission (black).

40-string configuration in this section and the next. The post-trial p-value is 29%, which is compatible with background fluctuations.

8. Triggered Searches Based on Intermittent Photon Observations

Ground based observatories such as H.E.S.S., MAGIC, and VERITAS cannot monitor sources continuously, because they can only operate when there is good nighttime visibility. Their observations are nevertheless extremely important for neutrino searches, because they detect photons at TeV energies that are potentially better correlated to neutrinos of

588 the energies to which IceCube is sensitive. While these observatories can issue an alert for
589 source activity, they often cannot constrain the beginning or end of the activity to within
590 a few days. For alerts such as these, the present analysis uses a simple time cut, taking a
591 window for events one day before and after the identified flare. The catalogue corresponding
592 to the 40-string data includes a recent suspect "orphan flare" at the level of 10 Crab from
593 Mrk 421 observed by VERITAS and MAGIC (Collaboration et al. 2009; Wagner et al.
594 2009).

595 ### 8.1. Method and Expected Performance

596 The nature of this analysis is a simple cut in time between t_{min} and t_{max}, which can be
597 expressed as:

$$S_i^{time} = \frac{H(t_{max} - t_i) \times H(t_i - t_{min})}{t_{max} - t_{min}} \tag{11}$$

598 where t_i is the arrival time of the event, t_{max} and t_{min} are the upper and lower bounds
599 of the time window defining the flare, and H is the Heavyside step function. This time
600 dependent signal pdf is then used in eq. 4.

601 ### 8.2. Results

602 Five of the seven flares tested with the 22 string data (Tab. 3) found no excess of events
603 in the vicinity of the tested sources in the selected time windows, while S5 0716+71 and
604 1ES 1959+650 showed one event each. The post-trial p-value is 14%, the most significant
605 flare being the 10 day flare of S5 0716+71. This result is consistent with background
606 fluctuations.

Of the six sources tested with the 40-string data (Tab. 4), five showed no excess of events in the vicinity of the sources during the selected time periods. The final post-trial p-value for the 40 string analysis (considering the 15 flares in Tab. 2 and Tab. 4) is 29%.

9. Conclusions

In this paper we discuss four time-dependent searches: two are "untriggered" and scan the entire parameter space of direction, energy and time to look for clusters of neutrino events; the others are "triggered" by multi-wavelength information. While the first two searches are generic and sensitive to flares not seen in photons, the others are more sensitive because of the reduced trial factor but concern specific catalogues of variable sources. Time dependent searches can be more sensitive to short flares thanks to the reduction of the background of atmospheric muons and neutrinos over short time scales. The untriggered search for a predefined catalogue of variable sources shows a post-trial p-value of 95% and upper limits on the fluence are calculated (see Tab. 1). The all-sky scan over all directions finds that the most significant cluster of events is separated in time by 22 s and in space by 2^o and has a p-value of 56%. The most significant flare between catalogues compiled using Fermi-LAT and IACT alerts during the 40-string configuration data taking is PKS 1502+106, with a p-value of 29% after trials. The most significant flare during the 22-string configuration is S5 0716+71 with a p-value of 14% after trials. These results are compatible with a fluctuation of the background.

We acknowledge the support from the following agencies: U.S. National Science Foundation-Office of Polar Program, U.S. National Science Foundation-Physics Division, University of Wisconsin Alumni Research Foundation, the Grid Laboratory Of Wisconsin (GLOW) grid infrastructure at the University of Wisconsin - Madison, the Open Science

Grid (OSG) grid infrastructure; U.S. Department of Energy, and National Energy Research Scientific Computing Center, the Louisiana Optical Network Initiative (LONI) grid computing resources; Swedish Research Council, Swedish Polar Research Secretariat, and Knut and Alice Wallenberg Foundation, Sweden; German Ministry for Education and Research (BMBF), Deutsche Forschungsgemeinschaft (DFG), Germany; Fund for Scientific Research (FNRS-FWO), Flanders Institute to encourage scientific and technological research in industry (IWT), Belgian Federal Science Policy Office (Belspo); the Netherlands Organisation for Scientific Research (NWO); M. Ribordy acknowledges the support of the SNF (Switzerland); A. Kappes and A. Groß acknowledge support by the EU Marie Curie OIF Program.

Source	dec [°]	ra [°]	log E_{min} (GeV)	log E_{max} (GeV)	pre-trial p-value	Best-Fit Threshold (10^{-6} cm^{-2} s^{-1})	Duration (days)	Upper limit (GeV/cm^2)
PKS 1510-089	-9.09	228.19	4.80	7.79	—	0	282	2.49
3C 66A/B	43.04	35.65	3.28	5.73	0.47	0.675	57	0.778
3C 454.3	16.15	343.50	3.58	6.34	0.20	9.47	2.5	0.422
PKS 1454-354	-35.64	224.41	5.64	7.82	—	0	282	13.1
3C 279	-5.8	194.03	4.18	7.63	0.47	2.34	6	1.69
PKS 0454-234	-23.43	74.29	5.49	7.87	—	0	282	7.87
PKS 1502+106	10.51	226.12	3.68	6.58	0.049	3.13	8	0.370
J123939+044409	4.7	189.9	3.74	7.07	—	0	282	0.661

Table 2:: Sources tested with the 40 string data and pre-trial p-values for the flare search with continuous lightcurves. In the event of an underfluctuation no p-value is calculated. The overlap between the Fermi public release data and the 40-string data taking period is 282 days. The duration column corresponds to the amount of time for the lightcurve which is above the best-fit threshold.

Source	dec [°]	ra [°]	Alert Ref.	Time Window (MJD)	log E_{min} (GeV)	log E_{max} (GeV)	p-value (pre-trial)	Fluence Limit (GeV/cm^2)
1ES 1959+650	65.1	300.1	(Bottacini et al. 2007)	54428-54433	3.09	5.39	—	1.78
1ES 1959+650	65.1	300.1	(Whipple 2007)	54435.5-54440.5	3.09	5.39	0.08	1.81
3C 454.3	16.2	343.5	(Vercellone et al. 2008)	54305-54311	3.76	6.45	—	0.812
3C 454.3	16.2	343.5	(Vercellone et al. 2009)	54416-54426	3.76	6.45	—	0.812
Cyg X-1	35.2	299.5	(Golenetskii et al. 2007)	54319.5-54320.5	3.43	5.96	—	1.19
S5 0716+71	71.3	110.5	(Chen, A. W. et al. 2008)	54350-54356	3.06	5.31	—	2.00
S5 0716+71	71.3	110.5	(Chen, A. W. et al. 2008)	54392-54402	3.06	5.31	0.02	2.00

Table 3:: Flare list during the 22 strings data-taking: source name, references for the alert, interval in modified julian day, pre-trial p-value. The p-value is calculated only when $\hat{n}_s$ is greater than zero.

Source	dec [°]	ra [°]	Alert Ref.	Time Window (MJD)	$\log E_{min}$ (GeV)	$\log E_{max}$ (GeV)	p-value (pre-trial)	Fluence Limit (GeV/cm^2)
Markarian 421	38.2	166.1	(Pichel 2009)	54586-54592	3.31	5.81	—	1.51
			(Vittorini et al. 2009)	54621-54631				
W Comae	28.2	185.4	(Acciari et al. 2009)	54623-54627	3.43	5.99	—	1.32
S5 0716+714	71.3	110.5	(Mazin et al. 2009)	54572-54582	2.99	5.26	0.34	3.26
SGR 0501+4516	45.3	75.3	(Rea et al. 2009)	54700-54706	3.23	5.70	—	1.72
1ES 1218+304	30.2	185.3	(Acciari et al. 2010)	54859-54864	3.42	5.97	—	1.43
Markarian 501	39.8	253.5	(Pichel 2009)	54951-54953	3.32	5.77	—	1.78

Table 4:: Flare list seen with occasional coverage during the 40-string data-taking. References are for the alert which prompted the selection. The p-value is calculated only when $\hat{n}_s$ is greater than zero. The flare windows for Markarian 421 were added together, only one p-value and upper limit for both periods is calculated.

REFERENCES

Abbasi, R., et al. 2009a, Phys. Rev. Lett., 103, 221102

—. 2009b, Astrophys. J., 701, L47

—. 2009c, Astrophys. J., 701, 1721

—. 2009d, Nucl. Instrum. Meth., A601, 294

—. 2010a, Nucl. Instrum. Meth., A618, 139

—. 2010b, *Measurement of the atmospheric neutrino energy spectrum from 100 GeV to 400 TeV with IceCube*, in preparation

—. 2010c, Astrophys. J., 710, 346

—. 2010d, *Searches for muon neutrino emission from gamma ray bursts with IceCube 40 string detector*, in preparation

—. 2010e, *Time-Integrated Searches for Point-like Sources of Neutrinos with 40 Strings of IceCube*, in preparation

Abdo, A. A., & Collaboration, f. t. F.-L. 2010, Astrophys. J., 715, 429

Abdo, A. A., et al. 2009a, Astrophys. J., 699, 817

—. 2009b, Astrophys. J. Suppl., 183, 46

Acciari, V. A., et al. 2009, Astrophys. J., 707, 612

—. 2010, Astrophys. J., 709, L163

Achterberg, A., et al. 2006a, Astropart. Phys., 26, 155

—. 2006b, Phys. Rev. Lett., 97, 221101

660 —. 2006c, Astropart. Phys., 26, 282

661 —. 2007a, Phys. Rev., D76, 027101

662 —. 2007b, Phys. Rev., D75, 102001

663 Aharonian, F. 2007, Astrophys. J., 664, L71

664 Albert, J., et al. 2007, Astrophys. J., 669, 862

665 Bazo-Alba, J. L., Bernardini, E., & Lauer, R. 2009, in Proc. of the 31st Int. Cosmic Ray
666 Conf, Lodz, Poland, arXiv:0908.4209

667 Bernardini, E., et al. 2005, Presented at Workshop on Particles and Radiation from Cosmic
668 Accelerators, Chiba, Japan, http://www.astro.phys.s.chiba-u.ac.jp/ca2005/

669 Blazejowski, M., et al. 2005, Astrophys. J., 630, 130

670 Boettcher, M. 2007, Astrophys. Space Sci., 309, 95

671 —. 2010, *Models for the Spectral Energy Distributions and Variability of Blazars*,
672 arXiv:1006.5048

673 Boettcher, M., Reimer, A., & Marscher, A. P. 2009, AIP Conf. Proc., 1085, 427

674 Bottacini, E., et al. 2007, The Astronomers Telegram, 1315, 1

675 Braun, J., et al. 2008, Astropart. Phys., 29, 299

676 —. 2010, Astropart. Phys., 33, 175

677 Chen, A. W. et al. 2008, A&A, 489, L37

678 Ciprini, S. 2008, The Astronomer's Telegram, 1650, 1

679 Ciprini, S., Abdo, . A. A., & collaboration, T. M. C. 2010, Astrophys. J., 710, 810

680 Collaboration, T. V., Perez, I. d. l. C., Ibarra, A., Rodriguez, P., & Collaboration, T. M.
681 2009, Astrophys. J., 703, 169

682 Gaidos, J. A., et al. 1996, Nature, 383, 319

683 Golenetskii, S., et al. 2007, GCN Circulars, 6745

684 Halzen, F., & Hooper, D. 2005, Astropart. Phys., 23, 537

685 Halzen, F., Landsman, H., & Montaruli, T. 2005, *TeV photons and neutrinos from giant*
686 *soft-gamma repeaters flares*, arXiv:astro-ph/0503348

687 Horan, D., et al. 2009, Astrophys. J., 695, 596

688 Ioka, K., Razzaque, S., Kobayashi, S., & Meszaros, P. 2005, Astrophys. J., 633, 1013

689 Kartaltepe, J. S., & Balonek, T. J. 2007, Astron. J., 133, 2866

690 Krawczynski, H., et al. 2004, Astrophys. J., 601, 151

691 Kumar, H. S., Ibrahim, A. I., & Safi-Harb, S. 2010, Astrophys. J., 716, 97

692 Liu, X.-W., Wu, X.-F., & Lu, T. 2010, New Astron., 15, 292

693 Mazin, D., Lindfors, E., Berger, K., Galante, N., Prandini, P., & Saito, T. 2009, in *Discovery*
694 *of Very High Energy -rays from the famous blazar S5 0716+714* Proc. of the 31st
695 Int. Cosmic Ray Conf,, Lodz, Poland

696 Mereghetti, S. 2008, Astron. Astrophys. Rev., 15, 225

697 Meszaros, P. 2006, Rept. Prog. Phys., 69, 2259

698 Meszaros, P., & Rees, M. J. 1993, Astrophys. J., 405, 278

699 Neyman, J., & Pearson, E. S. 1933, Phil. Trans. R. Soc. Lond. A, 231, 289

Pichel, A. 2009, in *Highlights from the Whipple 10-m VHE Blazar Monitoring Program* Proc. of the 31st Int. Cosmic Ray Conf,, Lodz, Poland, arXiv:0908.0010

Piran, T. 2004, Rev. Mod. Phys., 76, 1143

Rea, N., et al. 2009, *The first outburst of the new magnetar candidate SGR 0501+4516* arXiv:0904.2413

Reimer, A., Bottcher, M., & Postnikov, S. 2005, Astrophys. J., 630, 186

Resconi, E., Franco, D., Gross, A., Costamante, L., & Flaccomio, E. 2009, Astron. Astrophys., 502, 499

Satalecka, K., Bernardini, E., Ackermann, M., & Tluczykont, M. 2007, in Proc. of the 30th Int. Cosmic Ray Conf., Mérida, Yucatán, México, 115–118, arXiv:0711.0353v1

Scargle, J. D. 1998, Astrophys. J, 504, 405

Tilav, S., et al. 2009, in Proc. of the 31st Int. Cosmic Ray Conf, Lodz, Poland, *Atmospheric Variations as observed by IceCube*, arXiv:1001.0776

Vercellone, S., et al. 2008, Astrophys. J, 676, L13

—. 2009, Astrophys. J., 690, 1018

Vittorini, V., et al. 2009, Astrophys. J., 691, L13

Wagner, R. M., et al. 2009, Proc. of 31^{th} Int. Cosmic Ray Conf, 0926

Waxman, E. 2003, Lect. Notes Phys., 598, 393

Whipple. 2007, http://veritas.sao.arizona.edu/documents/summary1es1959.table